Available online at www.sciencedirect.com

SciVerse ScienceDirect

Journal of the European Ceramic Society 32 (2012) 2765–2775

www.elsevier.com/locate/jeurceramsoc

Bioactivity modulation of Bioglass® powder by thermal treatment

Marlin Magallanes-Perdomo [a,b], Sylvain Meille [a,b], Jean-Marc Chenal [a,b], Elodie Pacard [c], Jérôme Chevalier [a,b,*]

[a] Université de Lyon, CNRS, France
[b] INSA-Lyon, MATEIS UMR5510, F-69621 Villeurbanne, France
[c] Noraker, 13 Avenue Albert Einstein, 69100 Villeurbanne, France

Available online 10 April 2012

Abstract

A discussion of the effects of Bioglass® powder crystallisation on the in vitro bioactivity in simulated body fluid (SBF) is presented.

Starting from Bioglass® powder, different glass–ceramics were obtained by thermal treatments between 580 °C and 800 °C, with variable crystallisation content (from 10 to 92 wt%). All samples (glass and glass–ceramics) showed apatite formation at their surface when immersed in SBF. In case of the glass and the samples with lowest crystallinity, the first step of apatite formation involved a homogenous dissolution followed by an amorphous calcium phosphate (CaP) layer precipitation. For the samples with a high crystallisation content, heterogeneous dissolution occurred. For the first time, the Stevels number of the amorphous phase is used to explain the possible dissolution of the crystalline phase present in materials with a similar chemical composition of the Bioglass®. All samples presented at 21 days of immersion in SBF B-type hydroxycarbonate apatite crystals.

Keywords: Simulated body fluid; Glass–ceramics; Apatite; Glass; Biomedical applications

1. Introduction

The first bioactive biomaterial was developed by Hench et al. in 1969.[1,2] It consists of a silicate network glass incorporating sodium, calcium and phosphorus ions, known as Bioglass®. The ability of this glass to bond to both soft and hard tissues through a hydroxyapatite layer formation has been widely documented. Its ability to promote bone growth due to stimulatory effects of the ionic products of Bioglass® dissolution on human osteoblast proliferation has also been demonstrated.[3,4]

Current applications of the 45S5 Bioglass® are in the form of dense pieces for small bone replacement[5,6] or as particles larger than 100 μm diameters as bone regenerative materials.[7–10] Other applications are foreseen today in tissue engineering as large scaffolds or as reinforcing agents of polymer matrix composites.[11–22]

The manufacturing of scaffolds from Bioglass® particles comprises a sintering step that produces structural transformation of the particles. The challenge in development of these materials is to obtain a good compromise between crystallisation content, pore size (micro and macro-porosity), mechanical properties and bioactivity. The use of Bioglass® like filler in association with resorbable polymers to produce resorbable bioactive composites has emerged recently due to its osteoconductive and its osteoinductive properties.[11–18] It is known, however, that during elaboration of the composite, Bioglass® particles accelerates the degradation of hydrolysable polymers especially due to the release of alkaline ions that catalyses the polymer hydrolysis. This causes a decrease in the mechanical properties of the final product.[19] Different ways can be proposed to decrease the release of alkaline ions (changes the chemical composition of the glass,[23] surface functionalisation by cleaning and silanisation methods[24]). In the present investigation a thermal treatment of Bioglass® particles before mixing to the polymer has been proposed to decrease the leaching of ions. Such decrease in ion leaching should be beneficial to the composite structural integrity, because it should limit the high dissolution rate of the filler, increasing the mechanical properties during in vivo implantation (since low dissolution rate can

* Corresponding author at: Université de Lyon, CNRS, Villeurbanne, France. Tel.: +33 04 72 43 61 25; fax: +33 04 72 43 85 28.
E-mail addresses: marlinmagallanes@hotmail.com (M. Magallanes-Perdomo), jerome.chevalier@insa-lyon.fr (J. Chevalier).

0955-2219/$ – see front matter © 2012 Elsevier Ltd. All rights reserved.
doi:10.1016/j.jeurceramsoc.2012.03.018

produce a rapprochement between implant dissolution and new bone formation rate).

A thermal treatment on Bioglass® particles to make scaffolds or crystallised particles involves structural transformations that could modify the release of ions and therefore bioactivity. It is therefore important to assess that the particles after crystallisation still remains sufficiently bioactive.

Most of the existing literature on the effect of crystallisation on the bioactivity of the Bioglass® in simulated body fluid (SBF) focuses on the studies of dense pieces or scaffolds.[25–28] The investigations reveal that the presence of crystalline phase slightly decreased the kinetics but did not suppress the formation of a hydroxyapatite layer in SBF, which is considered as a marker for bioactivity.[20] According to our knowledge, no other systematic work relating to powder sample treated at different temperatures is available.

Here, the effect of Bioglass® powder crystallisation content by thermal treatment between 580 °C and 800 °C (to obtain different crystallisation content and nature of crystalline phases[29,30]) on the in vitro bioactivity mechanism in SBF is presented. For this, powders after thermal treatment were immersed in SBF for different time between 2 h and 21 days. The solutions were examined for changes in the concentration of Ca, Si, P and Na ions using inductively coupled plasma atomic emission spectroscopy (ICP-AES). Afterwards, the characterisations of the specimens were carried out by scanning electron microscopy (SEM), FT-IR spectroscopy and X-ray diffraction.

The possible impact of this work in the bone replacement sector or/and in bone engineering is focused on the tailoring of Bioglass® derived filler by thermal treatments, allowing for example the implant design with gradients of properties.

2. Materials and methods

2.1. Bioglass® glass powder preparation

Bioglass® powder was obtained by a melt-quenching route. The chemicals used for the synthesis of these particles were reagent-grade calcium carbonate ($CaCO_3$), sodium carbonate (Na_2CO_3), high-purity quartz (SiO_2) and high-purity phosphorus oxide (P_2O_5).

The mixed powders were melted for 4 h in a Pt crucible at 1400 °C with a decarbonation step of 5 h at 950 °C. The molten glass was poured in water to obtain a frit that was then ball milled in ethanol to obtain a fine powder with a mean size of 3.5 μm.

2.2. Glass–ceramics powder preparation

In previous studies, Lefebvre et al.[29,30] provided a precise understanding of the main transformation processes occurring during thermal treatment of Bioglass® particles. In these studies, the crystallisation kinetics of the major phase ($Na_2CaSi_2O_6$) was established by temperature–time–transformation (T–T–T) curves. Based on these T–T–T curves and taking into account the quantity and crystalline phases present, so as the formation of necks between the particles, different thermal treatments were proposed to obtain different crystallisation content, as shown in Table 1, with temperature higher than the glass transition (550 °C).[29]

The thermal treatments were conducted with the following procedure: the samples were loaded into a small platinum foil crucible and then heated in air at 5 °C min^{-1} up to the temperature indicated in Table 1, holding this temperature for the time specified. Subsequently, the samples were cooled to room temperature at 5 °C min^{-1}. A first de-agglomeration was done in agate mortar, and then the samples were ground in wet state (with ethanol) using agate balls of 20 mm diameter. The milling time was between 45 and 30 min at 300 rpm to obtain a final mean particle size close to 4 μm.

2.3. Characterisation of the glass–ceramics and parent glass

2.3.1. Phase identification and quantitative analysis

XRD patterns were recorded on a Bruker Advance D8 diffractometer (Karlsruhe, Germany), between 10° and 60° (2θ) with 0.03° steps, counting for 15 s per step using CuK_α radiation. All samples were rotated at 0.25 rps during acquisition of patterns in order to improve powder averaging, which is essential with a view to obtaining accurate intensities and hence phase analyses. The X-ray tube was operated at 40 kV at 40 mA. The EVA-version 6.0 Diffrac plus software (Bruker AXS GmbH, Karlsruhe, Germany) was used to evaluate the patterns.

The quantitative analysis of the phases present in the samples after thermal treatment (including the amorphous content) was performed by the Rietveld quantitative amorphous content analysis (RQACA).[31] Considering a standard free of amorphous phases, RQACA relates the overall amorphous content to the overestimation of the internal crystalline standard in the Rietveld refinement. The overall amorphous phase content of the samples was derived from the refined CaF_2 phase ratios and the phase fractions of the crystalline components obtained directly in the Rietveld study were recalculated by taking into account the overall non-diffracting fraction. To do so, the samples were mixed with CaF_2 as internal standard, the final mixture contained 70.0 wt% treated glass and 30.0 wt% CaF_2. GSAS (general structure analysis system) suite program was used to refine the powder pattern by Rietveld analysis.

2.3.2. Morphological studies

The morphology of the samples was studied by high resolution field emission scanning electron microscopy (SEM, Zeiss Supra® 55VP). The samples were placed on adhesive carbon tabs (Agar, Stansted, England) and observed at low voltage (2 kV) without any gold coating.

The reported values of the layer thickness formed onto the surface were the average of five different sites for the same layer.

2.3.3. Structural studies

The changes in the surface of the powder after thermal treatment were studied by FT-IR spectroscopy in attenuated total reflectance (ATR) conditions, using Nicolet iS10 FTIR spectrometer equipped with a diamond HATR (Thermo Scientific Instrument, Wisconsin, U.S.A.). The resolution was 4 cm^{-1} and

Table 1
Phase composition of the treated samples from full quantitative Rietveld analysis and some refinement results for the samples mixed with CaF_2.

		Thermal treatment		
		580 °C-100 min	630 °C-25 min	800 °C-5 min
Quantitative analysis (wt%)	$Na_2CaSi_2O_6$	10.0 ± 0.4	80.0± 0.5	91.0 ± 0.7
	$Na_2Ca_4P_2SiO_{12}$	–	–	1.0 ± 0.3
	Amorphous phase	90.0 ± 0.7	20.0 ± 0.3	8.0 ± 0.3
Rietveld refinement (GSAS) discrepancy values	R_{wp}	9.0	8.2	9.1
	R_f Standard	5.8	4.2	5.8
	R_f $Na_2CaSi_2O_6$	7.7	8.8	4.5
	R_f $Na_2Ca_4P_2SiO_{12}$	–	–	8.9

the measurement range of 4000 and 500 cm^{-1}, with 32 scans per spectra.

2.4. Bioactivity in static simulated body fluid in static conditions (SBF)

The preparation of the SBF was carried out following the procedure reported in the ISO standard: 23317.[32] The powder samples (50 mg) were placed in a plastic container with 50 ml of SBF, corresponding to final concentration of 1 mg sample per ml of the SBF. The samples were kept immersed for different periods of time between 1 h and 21 days at 36.5 °C in an orbital shaker incubator Innova®40 (New Brunswick Scientific, NJ, U.S.A.) with an agitation rate of 120 rpm. After each time point, the filtration of the solution was carried out to recover the powder. This was studied by XRD, FT-IR spectroscopy and SEM, as described before.

The changes in the concentration of Ca, Si, P and Na ions in SBF solutions were examined using ICP-AES Optima 5300 DV (PerkinElmer, MA, U.S.A.).

3. Results

3.1. Glass and glass–ceramics characterisation before bioactivity studies

SEM pictures of the particles before bioactivity studies, Fig. 1, show that the roundness of the particles increases with the temperature of the thermal treatment.

The results of RQACA from the heat-treated samples are summarised in Table 1. This shows the phase evolution with temperature at 580, 630 and 800 °C with a holding time of 100, 25 and 5 min respectively. The values of the pattern-dependent disagreement factor (R_{WP}) were evaluated, and are listed in Table 1 (bottom part). The values are smaller than 10%, indicating good fits.[33] Furthermore, the values of the phase-dependent disagreement factor (R_F) are quite small, indicating a satisfactory fit for each phase. The final phase compositions for the three samples from the RQACA are given in Table 1 (top part).

All samples after thermal treatments presented $Na_2CaSi_2O_6$ as crystalline phase, only the treated sample at 800 °C also presented a small amount of $Na_2Ca_4P_2SiO_{12}$ (silicorhenanite), in agreement with Lefebvre et al.[29]

For simplicity in throughout the text, the samples are identified as 10, 80 and 92 wt% of crystallinity for the sample treated at 580 °C-100 min, 630 °C-25 min and 800 °C-5 min respectively.

Not only the amount of crystalline phase increases with thermal treatment, but the composition of the residual amorphous phase also changes.[34,35] This was calculated from the weight percentages of crystalline phases, as determined by Rietveld refinements, and the composition of the original glass. It must be noted that Si and Na ions of main crystalline phase ($Na_2CaSi_2O_6$) can be partially replaced, and therefore two different compositions of the major crystalline phase have been employed for the rational analyses: $Na_2CaSi_2O_6$ and $(Na_{0.951}Ca_{0.049})_2Ca(Si_{0.899}P_{0.101})_2O_6$ where sodium and silicon can be partially replaced by calcium and phosphorus respectively, as already noted in the litterature.[36]

Knowing the composition of the amorphous phase, its connectivity or Stevels number was calculated. According to Stevels model,[37] the silica-based glasses can be seen as inorganic polymers where the degree of polymerisation is determined by the concentration of network modifiers. The Stevels parameter (Y), expressing the mean number of the bridging oxygen ions (BO) per SiO_4 tetrahedron, is a useful way to describe the cross-linking of the glassy network. This parameter is readily calculated from the molar composition of the glass or of the amorphous phase of the glass–ceramic, using this equation:

$$Y = 2Z - 2R \quad (1)$$

where Z is the number of all types of oxygen per polyhedron and R is the ratio of the total number of oxygen ions to network forming element in the glass. The higher the number (Y), the more stable is the glass or the amorphous phase of the glass ceramic.[34,35,37] It was assumed that $Z = 4$, in agreement with ref. 37, and R is calculated from the concentration by two hypotheses (either main phase without P or with P). Two numbers are calculated, Table 2 shows the changes of the Stevels number of the amorphous phase with the crystallisation content of the samples. When the amount of crystals increases in the sample, the connectivity of the amorphous phase increases too.

The FT-IR spectra of the parent glass and the glass–ceramics are shown in Fig. 2. All samples presented bands in the region 1100–850 cm^{-1}: 1100–1000 cm^{-1}, associated with Si–O–Si stretching vibrational modes[26]; 950–900 cm^{-1}, related to Si–O-non-bridging oxygen bonds (NBO). These bands become much sharper due to the crystallisation process. The parent glass and

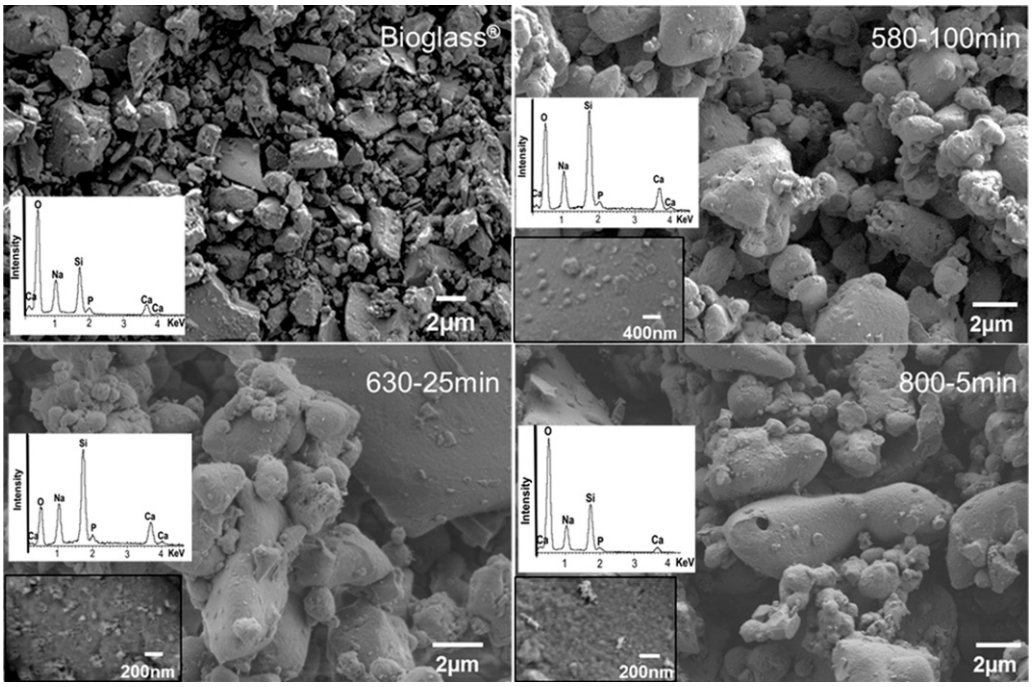

Fig. 1. Scanning electron micrograph of the particle surface before bioactivity studies in SBF.

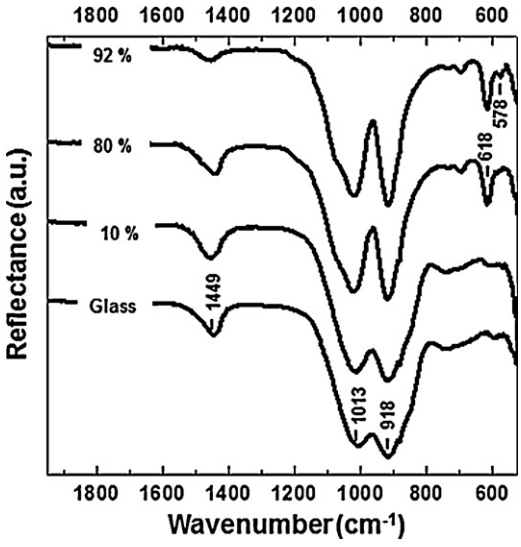

Fig. 2. FT-IR reflection spectra of the parent glass and glass–ceramics before soaking in SBF.

the treated samples presented also a peak at 1449 cm^{-1} related to the presence of carbonates. The samples with high crystallinity showed an additional band at 618 cm^{-1} corresponding to the main crystalline phase.[38] Only the sample with 92 wt% of crystalline phase showed one additional band at 578 cm^{-1} corresponding to P–O bending crystal, that can be attributed to the silicorhenanite phase.[28,39]

3.2. In vitro bioactivity studies

Fig. 3 illustrates the FT-IR reflection spectra of the glass and glass–ceramics before and after immersion in SBF. Clear changes can be noticed after immersion in SBF for all samples:

- In the first 2 h; four new bands are observed at 1250, 960–942, 800 and 580 cm^{-1}, the three first bands are associated to large surface of 3D silica structure (Si–O–Si, Si–OH or $Si–O^-$)[40–42] and the last one to amorphous calcium phosphate (CaP).[26] The band in the region 1110–950 cm^{-1} shifts to higher wavenumber. The bands at 1449 cm^{-1} and 918 cm^{-1} disappears.
- After 21 days of immersion; six new bands can be observed at approximately 1460, 1420, 1024, 872, 603 and 562 cm^{-1}. Bands at 1460, 1420, 872 cm^{-1} indicate the presence of CO_3^{2-} groups. The band observed at 1024 cm^{-1} is ascribed to symmetric vibration of P–O streching and the bands at 603 and 562 cm^{-1} are identified such as P–O bending crystal.[26,43]

The structural modifications observed after immersion of the samples in SBF, were accompanied with microstructural

Table 2
Variations of Stevels's number of the amorphous phase with the crystallisation content.

	Crystallisation content			
	0 wt% (glass)	10 wt% (580 °C)	80 wt% (630 °C)	92 wt% (800 °C)
Stevels's number of the amorphous phase	2.02	2.03–2.04	2.11–2.52	2.29–3.20

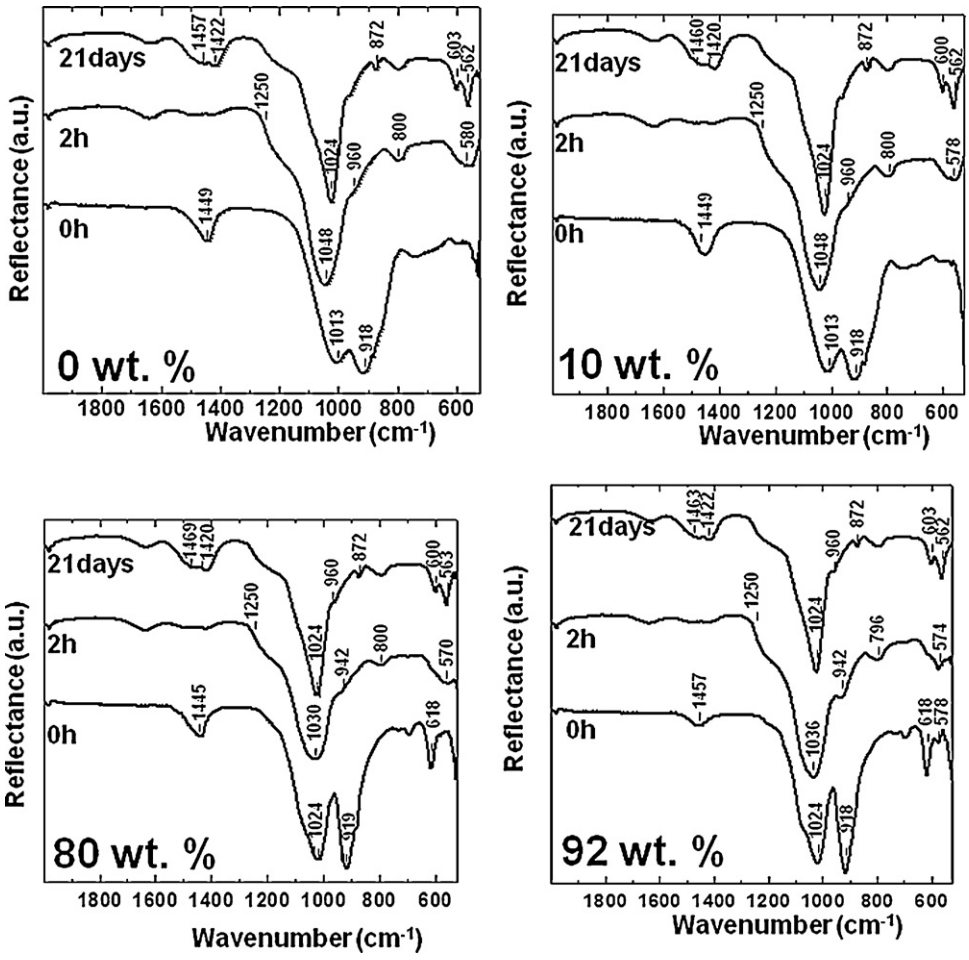

Fig. 3. FT-IR reflection spectrum of the parent glass and glass–ceramics after soaking in SBF for 2 h and 21 days. For comparison FT-IR results for the samples before immersion in SBF are also shown.

changes. The results can be divided into two groups: glass and low crystallinity glass–ceramic, and high crystallinity glass–ceramic.

3.2.1. Glass and low crystallinity glass–ceramic

For the glass sample in the first hour, a homogenous dissolution occurs, then a layer of amorphous CaP (wide band at approximately 600 cm^{-1} associated with P–O peaks from FT-IR results, Fig. 4) is formed onto the surface of the sample as observed by SEM. After 21 days of immersion, the layer increases in thickness (about 600 nm thick) and has crystalline structure, close to apatite.FT-IR results show that, after 21 days of study, the layer is like apatite with CO_3^{2-} ions in its structure (bands detected at 1460, 1420 and 875 cm^{-1}).[44,45]

For the sample with 10 wt% of crystallisation (Fig. 5) the results show a surface dissolution of the crystalline phase $Na_2CaSi_2O_6$ after 2 h of immersion in SBF. At the same immersion time, a layer covering the particles is detected by SEM, identified as amorphous CaP by FT-IR spectroscopy. As for the glass sample, when immersion time increases the thickness and the crystallinity of the layer increases. After 21 days in SBF, the layer is formed by hydroxycarbonate apatite crystals (about 500 nm thick).

3.2.2. High crystallinity glass–ceramics (above 80 wt%)

The results of SEM and XRD of the samples with 80 wt% of crystals after 2 h and 21 days are shown in Fig. 6. This sample presented a heterogeneous dissolution with a fragmentation of particles into small pieces. The XRD pattern shows a decrease of the intensity of the peak corresponding to $Na_2CaSi_2O_6$. This dissolution produced an increase of ions in the solution and then its saturation, leading to the formation of aggregates identified as amorphous CaP by FT-IR spectroscopy. These aggregates were crystalline for the samples immersed 21 days and identified as hydroxycarbonate apatite crystals.

The results for the sample with the highest crystallinity (92 wt%) are shown in Fig. 7. This sample presented a preferential dissolution of the crystalline phases, the XRD pattern shows a decrease of the intensity of the peak corresponding to $Na_2CaSi_2O_6$. After 2 h in SBF, a small amount of CaP aggregates was detected by FT-IR spectroscopy. These aggregates were crystalline for the samples immersed 21 days and also identified as hydroxycarbonate apatite crystals.

3.2.3. Other considerations of the in vitro behaviour

The experimental variation in calcium, silicon, sodium and phosphorus ions concentrations in SBF at 36.5 °C for 72 h of

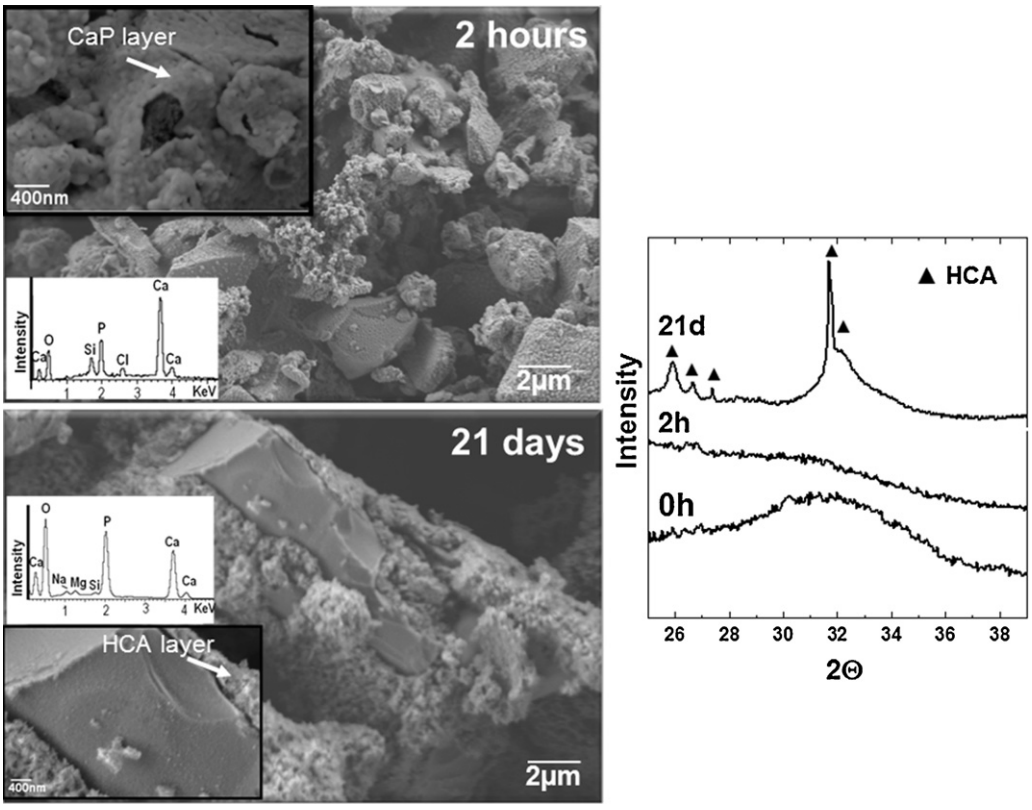

Fig. 4. Scanning electron micrographs and XRD of the Bioglass® after soaking in SBF for 2 h and 21 days. For comparison the XRD for the Bioglass® before immersion in SBF are also shown.

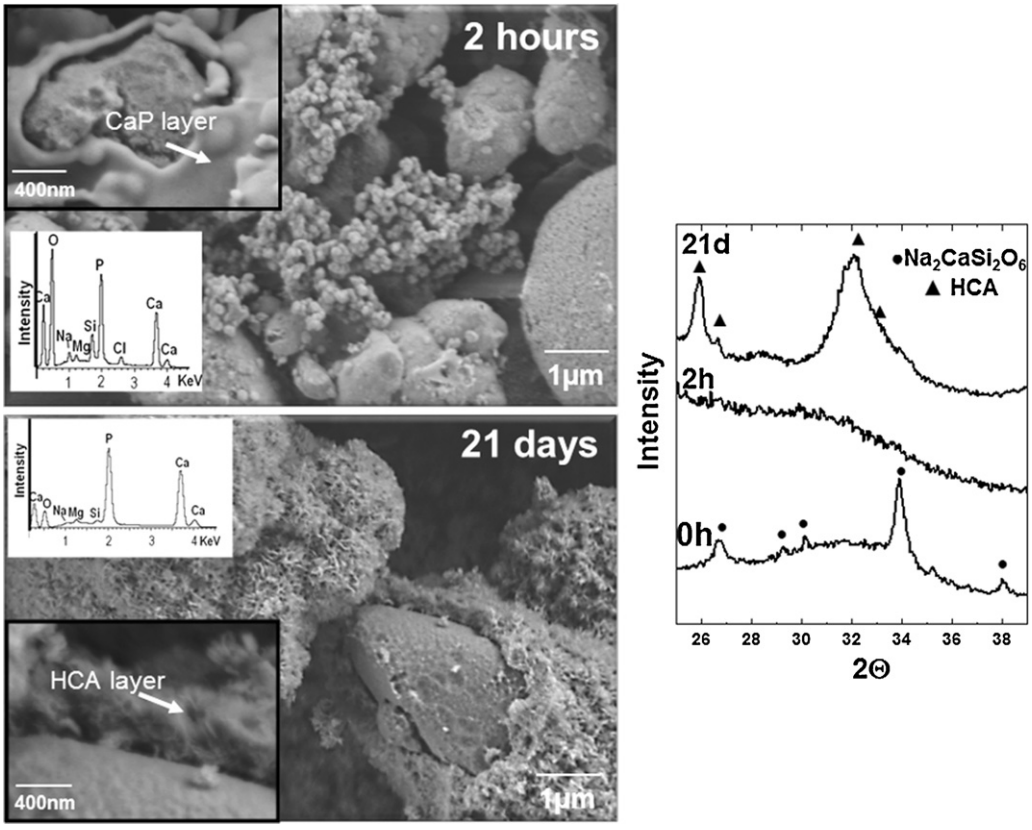

Fig. 5. Scanning electron micrographs and XRD of the sample with 10 wt% of crystalline phase after soaking in SBF for 2 h and 21 days. For comparison the XRD for sample before immersion in SBF are also shown.

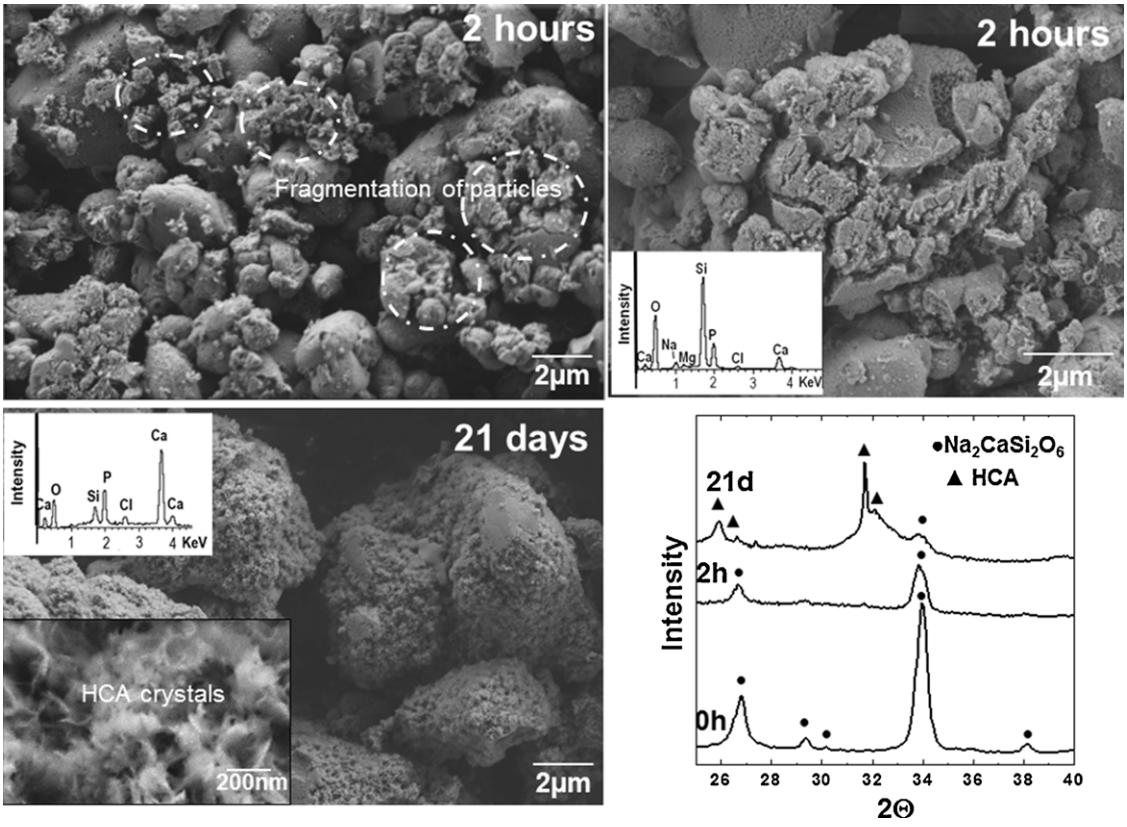

Fig. 6. Scanning electron micrographs and XRD of the sample with 80 wt% of crystalline phase after soaking in SBF for 2 h and 21 days. For comparison the XRD for sample before immersion in SBF are also shown.

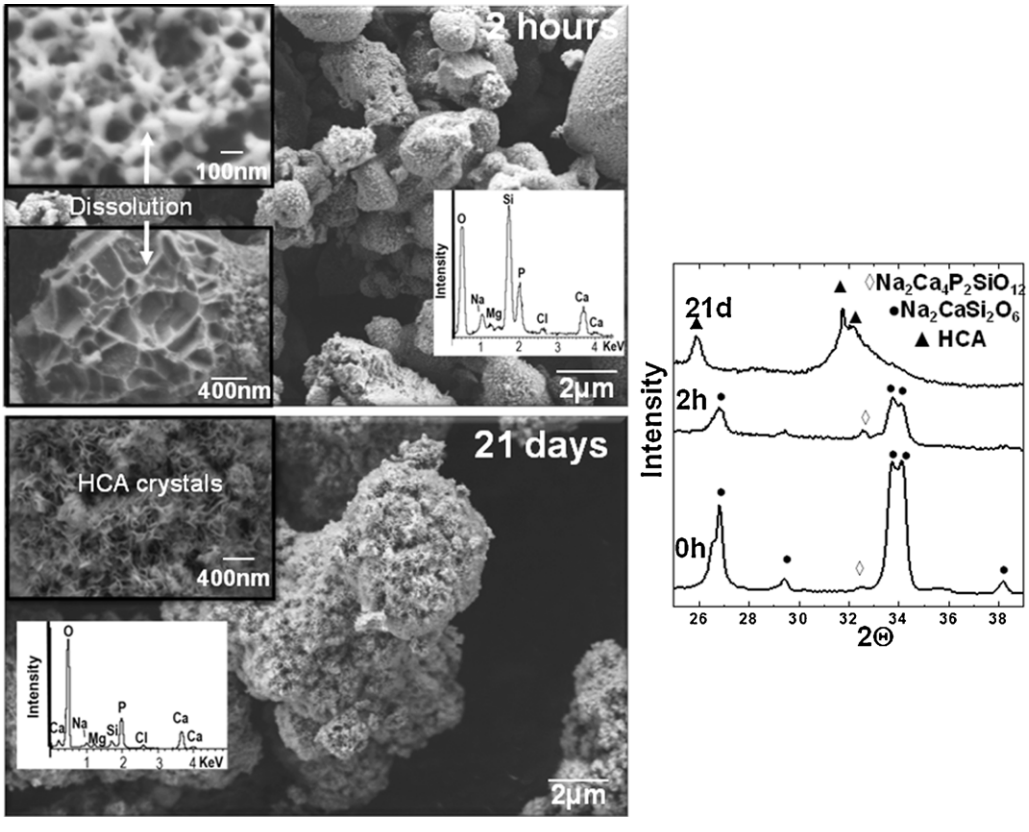

Fig. 7. Scanning electron micrographs and XRD of the sample with 92 wt% of crystalline phase after soaking in SBF for 2 h and 21 days. For comparison the XRD for sample before immersion in SBF are also shown.

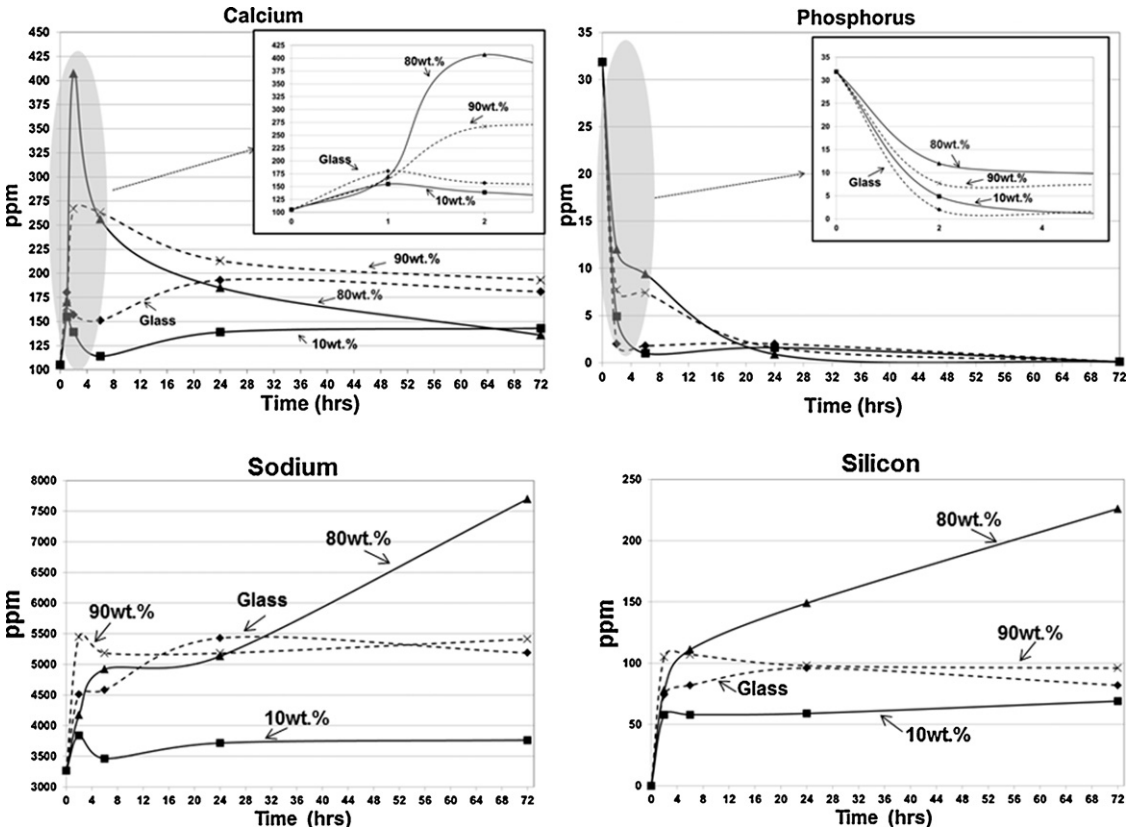

Fig. 8. Changes in calcium (Ca), phosphorus (P), sodium (Na) and silicon (Si) ions concentration with soaking time in SBF during in vitro test.

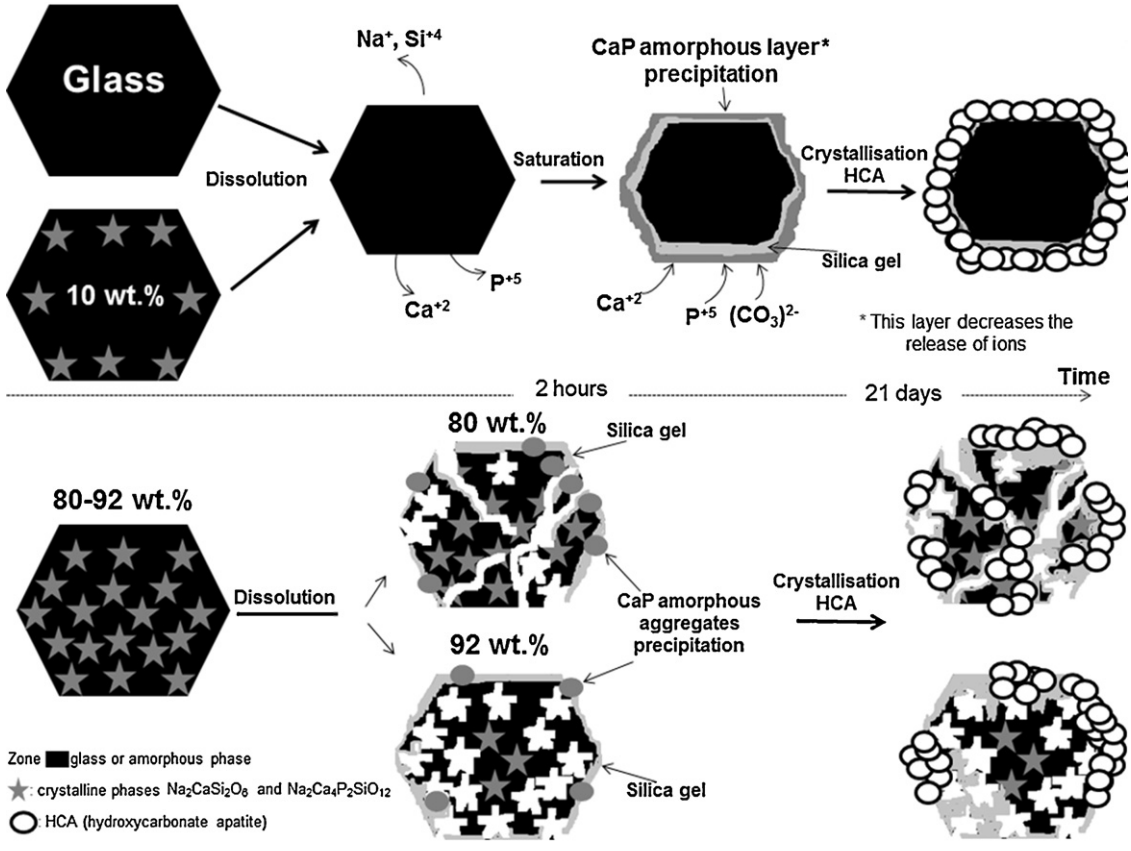

Fig. 9. Schematic mechanism of the formation of apatite for all samples in SBF.

immersion for glass and glass–ceramics samples is presented in Fig. 8.

The recorded changes in the concentration of the different ions showed that during the first stage of immersion, below 1 h, all samples released Si, Na and Ca ions. The concentrations of silicon and sodium stay nearly constant after 4 h, except for the sample with 80 wt% of crystallisation that continuously increased during the in vitro experiment, reaching 225 and 7800 ppm respectively after 72 h.

During the second stage of immersion, the Ca ions concentration decreased in the SBF in the course of 2 h of study for the glass and the sample with low crystallinity (10 wt%), and after 4 h for samples with high crystallinity.

The CaP layer formed into the surface of the glass and the sample with 10 wt% of crystals after 2 h of immersion, decreases the release of ions; this explains why after this period the concentration of sodium and silicon ions does not change for these two samples (Fig. 8).

The phosphorus concentration decreased for all samples studied in the course of 2 h, and remained at this level afterwards.

4. Discussion

4.1. Influence of thermal treatment in the structure of Bioglass®

When the Bioglass® was treated thermally at temperature higher than its glass transition temperature (550 °C),[29] it started to crystallise.

As determined by FT-IR, the parent glass and the sample with 10 wt% of crystallisation showed no significant structural differences, as already noted by Filho et al.[25] for a sample with a volume percentage of crystallisation close to 8%. This could explain the similar behaviour detected for the glass and for the sample with 10 wt% crystalline phase in SBF.

The carbonate peak detected for all samples at ~1449 cm^{-1} can be atmospheric CO_2 adsorbed and/or CO_2 dissolved in the melted during glass elaboration,[46,47] this peak has already been noticed in other studies on Bioglass®.[42]

The changes observed in the FT-IR spectra (Fig. 2) for the sample with 80 and 92 wt% of crystalline phase are linked to $Na_2CaSi_2O_6$ crystallisation. The FT-IR results obtained are close to the Peitl et al.[26] for samples with a composition near to 45S5 Bioglass® (47.5 SiO_2, 23.2 Na_2O, 23.2 CaO, 6.0 P_2O_5 wt%). In Peitl study, a fully crystallised sample without peak at 618 cm^{-1} (corresponding to phosphorus rich phase) was obtained, indicating that phosphorus ions remain in solid solution. An additional thermal treatment (17 h at 820 °C) was necessary to obtain a sample containing the phosphorus rich phase (silicorhenanite) with a peak at 618 cm^{-1} in the FT-IR spectra. In the present study, with a simple thermal treatment (5 min at 800 °C), it was possible to obtain samples with silicorhenanite. The difference with the previous study can be mainly attributed to the different morphology of the samples. Here, a sample with a 3.5 μm of mean size was used, in the study of Peitl a bulk sample was used. It is well know that when the size of the particles increases the kinetics of crystallisation decreases.[48] Lefebvre et al.[29] also observed silicorhenanite with a simple thermal treatment at 800 °C of a powder sample (1 μm), this being consistent with our results.

4.2. In vitro bioactivity studies

From the experimental data, the mechanism of apatite formation onto the different samples can be established (Fig. 9). The first five stages of bioactivity mechanism proposed by Cao and Hench[49] also are valid for the samples with higher content of crystallisation. During the first stages of the reaction, the high Ca concentration in the SBF solution (Fig. 8) enhances the nucleation of bone like apatite on the surface of the specimens. Then, the decrease in calcium and phosphorus ions concentration (Fig. 8) in all samples is due to the precipitation of an amorphous CaP on the particle surface. In the case of glass and low crystallinity samples, this forms a layer and for the samples with high crystallinity it forms isolated aggregates. This change in form of the CaP precipitates modifies the reactivity of the samples. In the first time (up to 2 h) the glass and the sample with low crystallinity presented the highest reactivity. Then, the formation of the CaP layer decreased the release of ions to SBF, decreasing its reactivity.

The change in reactivity of the samples in SBF is not only due to their level of crystallinity, but also to the chemical composition of the residual amorphous phase and particularly to its stability. The stability of the amorphous phase as determined by the Stevels number, increased with the crystallisation grade; this can explain why the sample with high crystallisation grade presented a preferential dissolution of the crystalline phase (Figs. 6 and 7).

In the present investigation, the Stevels model helps to explain the degradation of the crystalline phase, when glass–ceramics with Bioglass's composition were immersed in SBF. Other investigations [20,21] reported also that the crystalline phase dissolves first and explained this behaviour based on three phenomena: preferential dissolution of the crystal–amorphous interfaces, break of the particles into very fine due to structural defects, and amorphisation of the crystalline structure through ion exchange that produces point defects. In the present work, all these phenomena are not discarded, only the increased stability of the amorphous phase is added. In future works, complementary study of the treated sample will be done by nuclear magnetic resonance and transmission electron microscopy to determine exactly the location of the phosphorous in the sample and the Stevels number of the amorphous phase.

Also, with the results obtained in the present investigation, the Stevels number can be used to predict the bioactivity mechanisms of the Bioglass® powder with different crystallisation content.

It is important to note that all samples presented band at 799 and 960 cm^{-1} in the FT-IR spectra (Fig. 3) characteristic of a wet silica gel, also observed in sol–gel glasses.[40,44,50,51] It is well know that the formation of this silica gel is essential for the crystallisation of an apatite layer, therefore it is important for assessing the bioactive character of the material.[49–52]

From the SEM microstructure studies (Figs. 4–7), it is possible to note that this silica gel was in the form of layer in case of the glass and in the sample with low crystallisation grade, for the sample with higher crystallisation it is more like a 3D structure, resulting from the heterogeneous dissolution of the samples. It is not clear if the silica gel layer formation at the surface of the samples and the CaP precipitation are sequential steps or occurred at the same time, taking into account the high reactivity of the powder samples.The FT-IR spectra of all samples, after 21 days of immersion indicated the presence of B-type hydroxycarbonate apatite due to existence of these bands: 1457, 1422, 872 cm^{-1} (Fig. 3), that corresponds to the CO_3^{2-} group that replacing PO_4^{3-} groups.[53–55] Also, the lack of the band at 628 cm^{-1} that corresponds to O–H stretching indicated low crystallinity, in agreement with XRD results (Figs. 4–7).[56,57]

It is to note that in the present investigation the SBF studies have been conducted under static conditions (without change of the solution, for the ease of the experimental procedure, since it is a powder sample this makes it difficult the refreshing of the solution without losing material). It is clear that SBF ions and pH contribute to dissolution of crystalline phase and apatite formation.

4.3. The impact of thermal treatments on Bioglass® scaffolds and Bioglass®-polymer composites

The data indicate that Bioglass® scaffolds could remain bioactive after the sintering process, as has been demonstrated by several authors,[20–22,25] but the mechanisms of apatite formation change with the crystallisation content.

Crystallised Bioglass® particles to use like filler in composites maintain a significant release of ions that could degrade the polymer matrix, but it is not clear if the change of the mechanism of bioactivity has an effect in that degradation. In future work, composite with crystallised Bioglass® particles will be characterised to study if the degradation of polymers occurs.

5. Conclusions

All samples, glass and glass–ceramics, showed apatite formation when were immersed in SBF under static conditions. In the case of the glass and sample with the lowest crystallinity, the first step of apatite formation includes a homogenous dissolution followed by an amorphous CaP layer precipitation. Further incorporation of calcium, phosphate and carbonates ions cause the crystallisation of this layer. For the samples with high crystallisation grade, a trend towards a preferential dissolution of the crystalline phase occurs. This behaviour is explained by the increased stability of the amorphous phase with the crystal grade, as described by the Stevels number. The ions released by the dissolution produce the saturation of the SBF thus precipitating amorphous CaP. Then, with the incorporation of calcium, phosphate and carbonates ions, these aggregates crystallise into hydroxycarbonate apatite.

Acknowledgement

The authors wish to acknowledge “Fonds Unique Interministériel (FUI)” of France government for its financial support under project HOBBIT.

References

1. Hench LL. Bioceramics: from concept to clinic. *J Am Ceram Soc* 1991;**74**:1487–510.
2. Hench LL. The story of Bioglass®. *J Mater Sci Mater Med* 2006;**17**:967–78.
3. Hench LL, Splinter RJ, Allen WC, Greenlee TK. Bonding mechanisms at the interface of ceramic prosthetic materials. *J Biomed Mater Res* 1971;**5**:117–41.
4. Xynos ID, Edgar AJ, Buttery LD, Hench LL, Polak JM. Gene-expression profiling of human osteoblasts following treatment with the ionic products of Bioglass® 45S5 dissolution. *J Biomed Mater Res* 2001;**55**:151–7.
5. Hench LL, Wilson J, Merwin G. Bioglass® implants for otology. In: Grote JJ, editor. *Biomaterials in otology*. The Hague, Boston, London: Martinus Nijhoff Publishers; 1983. p. 62–9.
6. Stanley HR, Hall MB, Clark AE, King CJ, Hench LL, Berte JJ. Using 45S5 Bioglass cones as endosseous ridge maintenance implants to prevent alveolar ridge resorption: a 5-year evaluation. *Int J Oral Maxillofac Implants* 1997;**12**:95–105.
7. Low SB, King CJ, Krieger J. An evaluation of bioactive ceramic in the treatment of periodontal osseous defects. *Int J Periodontics Restorative Dent* 1997;**17**:358–67.
8. Froum SJ, Weinberg MA, Tarnow D. Comparison of bioactive glass synthetic bone graft particles and open debridement in the treatment of human periodontal defects. A clinical study. *J Periodontol* 1998;**69**:698–709.
9. Lovelace TB, Mellonig JT, Meffert RM, Jones AA, Nummikoski PV, Cochran DL. Clinical evaluation of bioactive glass in the treatment of periodontal osseous defects in humans. *J Periodontol* 1998;**69**:1027–35.
10. Vogel M, Voigt C, Gross UM, Müller-Mai CM. In vivo comparison of bioactive glass particles in rabbits. *Biomaterials* 2001;**22**:357–62.
11. Leonor IB, Sousa RA, Cunha AM, Reis RL, Zhong ZP, Greenspan D. Novel starch thermoplastic/Bioglass composites: mechanical properties, degradation behavior in vitro bioactivity. *J Mater Sci Mater Med* 2002;**13**:939–45.
12. Rezwan K, Chen QZ, Blaker JJ, Boccaccini AR. Biodegradable and bioactive porous polymer/inorganic composite scaffolds for bone tissue engineering. *Biomaterials* 2006;**27**:3413–31.
13. Guarino V, Causa F, Ambrosio L. Bioactive scaffolds for bone and ligament tissue. *Expert Rev Med Devices* 2007;**4**:405–18.
14. Ginsac N, Chevalier J, Chenal JM, Meille S, Hartmann D, Zenati R. Evaluation of a PDLLA/45S5 bioglass composite: mechanical and biological properties. *Ceram Eng Sci Proc* 2010;**30**:95–104.
15. Misra SK, Philip SE, Chrzanowski W, Nazhat SN, Roy I, Knowles JC, et al. Incorporation of vitamin E in poly(3-hydroxybutyrate)/Bioglass composite films: effect on surface properties and cell attachment. *J R Soc Interface* 2009;**6**:401–9.
16. Peitl O, Orefice RL, Hench LL, Brennan AB. Effect of the crystallization of bioactive glass reinforcing agents on the mechanical properties of polymer composites. *Mater Sci Eng A Struct* 2004;**372**:245–51.
17. Cannilo V, Chiellini F, Fabbri Sola A. Production of Bioglass® 45S5-Polycaprolactone composite scaffolds via salt-leaching. *Compos Struct* 2010;**92**:183–232.
18. Ginsac N, Chenal JM, Meille S, Zenati R, Hartmann D, Chevalier J. Crystallisation processes at the surface of polylactic acid-bioactive glass composites during immersion in simulated body fluid. *J Biomed Mater Res B Appl Biomater* 2011;**99B**:412–9.
19. Blaker JJ, Bismarck A, Boccaccini AR, Young AM, Nazhat SN. Premature degradation of poly(alpha-hydroxyesters) during thermal processing of Bioglass®-containing composites. *Acta Biomater* 2010;**6**:756–62.
20. Boccaccini AR, Chen Q, Lefebvre L, Gremillard L, Chevalier J. Sintering, crystallisation and biodegradation behaviour of bioglass-derived glass–ceramics. *Faraday Discuss* 2007;**136**:27–44.

21. Chen QZ, Thompson ID, Boccaccini AR. 45S5 Bioglass-derived glass–ceramic scaffolds for bone tissue engineering. *Biomaterials* 2006;**27**:2414–25.
22. Sanz-Herrera JA, Boccaccini AR. Modelling bioactivity and degradation of bioactive glass based tissue engineering scaffolds. *Int J Solids Struct* 2011;**48**:257–68.
23. Goel A, Kapoor S, Rajagopal RR, Pascual MJ, Kim HW, Ferreira JMF. Alkali-free bioactive glasses for bone tissue engeneering: a preliminary investigation. *Acta Biomater* 2012;**8**:361–72.
24. Verné E, Vitale-Brovarone C, Bui E, Bianchi CL, Boccaccini AR. Surface functionalization of bioactive glasses. *J Biomed Mater Res A* 2008;**90**:981–92.
25. Filho OP, LaTorre GP, Hench LL. Effect of crystallization on apatite-layer formation bioactive glass 45S5. *J Biomed Mater Res* 1996;**30**:509–14.
26. Peitl O, Zanotto ED, Hench LL. Highly bioactive P_2O_5–Na_2O–CaO–SiO_2 glass–ceramics. *J Non-Cryst Solids* 2001;**292**:115–26.
27. ElBatal FH, ElKheshen A. Preparation and characterization of some substituted bioglasses and their ceramic derivatives from the system SiO_2–Na_2O–CaO–P_2O_5 and effect of gamma irradiation. *Mater Chem Phys* 2008;**110**:352–62.
28. Chatzistavrou X, Zorba T, Kontonasaki E, Chrissafis K, Koidis P, Paraskevopoulos KM. Following bioactive glass behaviour beyond melting temperature by thermal and optical methods. *Phys Status Solidi A* 2004;**201**:944–51.
29. Lefebvre L, Chevalier J, Gremillard L, Zenati R, Thollet G, Bernache-Assolant D, et al. Structural transformation of biaoctive glass 45S5 with thermal treatments. *Acta Mater* 2007;**55**:3305–13.
30. Lefebvre L, Gremillard L, Chevalier J, Zenati R, Bernache-Assolant D. Sintering behaviour of 45S5 bioactive glass. *Acta Biomater* 2008;**4**:1894–903.
31. De La Torre AG, Bruque S, Aranda MAG. Rietveld quantitative amorphous content analysis. *J Appl Crystallogr* 2001;**34**:196–202.
32. ISO 23317, International Organization for Standardization, Switzerland, 2007.
33. Young RA. *The Rietveld method*. Oxford: University Press; 1993. p. 336.
34. Strnad Z. Role of the glass phase in bioactive glass–ceramics. *Biomaterials* 1992;**13**:317–21.
35. Höland W, Beall GH. *Glass–ceramic technology*. OH, United States of America: The American Ceramic Society; 2002.
36. Huang LC, Lin CC, Shen P. Crystallization and stoichiometry of crystals in $Na_2CaSi_2O_6$–P_2O_5 based bioactive glasses. *Mater Sci Eng A Struct* 2007;**452–53**:326–33.
37. Stevels JM. Glass considered as polymer. *The Glass Industry* 1954;**35**:69–72.
38. Bretcanu O, Chatzistavrou X, Paraskevopoulos K, Conradt R, Thompson I, Boccaccini AR. Sintering and crystallisation of 45S5 Bioglass® powder. *J Eur Ceram Soc* 2009;**29**:3299–306.
39. Smith BC. *Infrared spectral interpretation: a systematic approach*. Boca Raton, FL: CRC Press; 1999.
40. Matos MC, Ilharco LM, Almeida RM. The evolution of TEOS to silica gel and glass by vibrational spectroscopy. *J Non-Cryst Solids* 1992;**147**(48):232–7.
41. Almeida RM, Pantano CG. Structural investigation of silica gel films by infrared spectroscopy. *J Appl Phys* 1990;**68**:4225–32.
42. Cerruti M, Greenspan D, Powers K. Effect of pH and ionic strength on the reactivity of Bioglass® 45S5. *Biomaterials* 2005;**26**:1665–74.
43. LaTorre G, Hench LL. In: Adair JH, Casey JA, editors. *Characterization methods for the solid-solution interface in ceramic system*. Westerville, OH: American Ceramic Society; 1993.
44. Mami M, Lucas-Girot A, Oudadesse H, Dorbez-Sridi R, Mezahi F, Dietrich E. Investigation of the surface reactivity of a sol–gel derived glass in the ternary system SiO_2–CaO–P_2O_5. *Appl Surf Sci* 2008;**254**:7386–93.
45. Chang ML, Tanaka J. FT-IR study for hydroxyapatite/collagen nanocomposite cross-linked by glutaraldehyde. *Biomaterials* 2002;**23**:4811–8.
46. Pearce ML. Solubility of carbon dioxide and variation of oxygen ion activity in soda–silica melts. *J Am Ceram Soc* 1964;**47**:342–7.
47. Navarro JF. *El Vidrio (the glass)*. 3rd ed. Spain: Consejo Superior de Investigaciones Científicas (CSIC); 2003. p. 171–3 [in Spanish].
48. Xu XJ, Ray CS, Day DE. Nucleation and crystallization of $Na_2O{\cdot}2CaO{\cdot}3SiO_2$ glass by thermal analysis. *J Am Ceram Soc* 1991;**74**:909–14.
49. Cao W, Hench LL. Bioactive materials. *Ceram Int* 1996;**22**:493–507.
50. Sepulveda P, Jones JR, Hench LL. In vitro dissolution of melt-derived 45S5 and sol–gel-derived 58S Bioglass®. *J Biomed Mater Res* 2002;**61**: 301–11.
51. Mozafari M, Moztarzadeh F. Tahriri Investigation of the physico-chemical reactivity of a mesoporous bioactive SiO_2–CaO–P_2O_5 glass in simulated body fluid. *J Non-Cryst Solids* 2010;**356**:1470–8.
52. Hench L, Wheeler DL, Greenspan DC. Molecular control of bioactivity in sol–gel glasses. *J Sol–Gel Sci Technol* 1998;**13**:245–50.
53. Müller FA, Müller L, Caillard D, Conforto E. Preferred growth orientation of biomimetic apatite crystals. *J Cryst Growth* 2007;**304**:464–71.
54. Elliot JC. *Structure and chemistry of the apatite and other calcium orthophosphate, studies in inorganic chemistry*. Amsterdam: Elsevier; 1994.
55. Sprio S, Tampieri A, Landi E, Sandri M, Martorana S, Celotti G, et al. Physico-chemical properties and solubility behaviour of multi-substituted hydroxyapatite powders containing silicon. *Mater Sci Eng C* 2008;**28**:179–87.
56. Kumar GS, Girija EK, Thamizhavel A, Yokogawa Y, Kalkura SN. Synthesis and characterization of bioactive hydroxyapatite–calcite nanocomposite for biomedical applications. *J Colloid Interface Sci* 2010;**349**:56–62.
57. Ergun C. Effect of Ti ion substitution on the structure of hydroxylapatite. *J Eur Ceram Soc* 2008;**28**:2137–49.